ARCHIVES OF METALLURGY

Volume 45 2000 Issue 4

STANISŁAW DYMEK *, MAREK DOLLAR **, MIROSŁAW WRÓBEL *,
MAREK BLICHARSKI *

MICROSTRUCTURE AND MECHANICAL BEHAVIOUR OF A PRECIPITATION HARDENED Ni–25 wt.% Mo–8 wt.% Cr ALLOY

MIKROSTRUKTURA I WŁASNOŚCI MECHANICZNE UMACNIANEGO WYDZIELENIAMI STOPU Ni–25% cięż. Mo–8% cięż. Cr

The paper gives a broad characteristic of a nickel-based superalloy containing 25 wt.% Mo and 8 wt.% Cr with particular attention to morphology of the metastable, dispersed $Ni_2(Mo, Cr)$ phase. The influence of different variants of heat treatment on the microstructure and mechanical properties was investigated. The applied heat treatments comparised soaking at temperature range 1065°C to 1095 followed by conventional aging at 650°C for 24 to 72 hours and intermediate heat treatment at 760°C to 980°C preceded the aging at 650°C. The conventional aging leads to the formation of lenticular precipitates of the dispersed $Ni_2(Mo,Cr)$ phase. The intermediate heat treatment influenced the size of the ordered precipitates and thus mechanical properties of the alloy. The largest precipitates were produced when the aging at 650°C was preceded by annealing at 760°C, the precipitates size decreased with the increase of intermediate heat treatment temperature bringing about the decrease of the yield strength.

The influence of prolonged aging at 650°C on the microstructure and properties was investigated. The aging for 4000 hours did not cause the decomposition of the metastable $Ni_2(Mo, Cr)$ phase. The plastic deformation preceded the aging accelerated the decomposition of this phase on the mixture of the Ni_3Mo and Ni_4Mo-based phases.

It was shown that at relatively small deformation the presence of the ordered phase changes the mechanism of deformation from dislocation glide to the mechanical twinning. The development of microstructure and crystallographic texture during deformation do not depend substantially on the precipitates size. The deformation microstructure as well as texture was typical for the f.c.c. metals with low stacking fault energy.

The influence of temperature, strain rate and environment on mechanical properties was investigated. It was shown that the long-term exposure at 650°C led to the increase of the precipitates size and strength. The dramatic drop in 650°C dictility was observed upon testing in air. The good dictility in vacuum was preserved.

* WYDZIAŁ METALURGII I INŻYNIERII MATERIAŁOWEJ, AKADEMIA GÓRNICZO-HUTNICZA, 30-059 KRAKÓW, AL. MICKIEWICZA 30

** ILLINOIS INSTITUTE OF TECHNOLOGY, CHICAGO, ILLINOIS, IL 60616, USA

W pracy dokonano kompleksowej charakterystyki nadstopu niklu zawierającego 25% Mo oraz 8% Cr (% masowy) z uwzględnieniem morfologii, umacniającej ten stop dyspersyjnej metastabilnej fazy $Ni_2(Mo, Cr)$. Przebadano wpływ na strukturę i właściwości mechaniczne różnych wariantów obróbki cieplnej, polegającej na przesycaniu w wodzie z temperatur od 1065 do 1095°C z konwencjonalnym starzeniem w temperaturze 650°C przez 24 do 72 godziny oraz poprzedzającym starzenie wyżarzaniem w temperaturach 760–980°C (obróbka pośrednia). Stwierdzono, że konwencjonalne starzenie prowadzi do utworzenia soczewkowych wydzieleń fazy $Ni_2(Mo,Cr)$ o wielkości około 10–20 nm. Obróbka pośrednia wpływa na wielkość wydzieleń fazy $Ni_2(Mo,Cr)$ i na własności mechaniczne stopu. Największe wydzielenia otrzymano po wyżarzaniu w 760°C; ze wzrostem temperatury wielkość wydzieleń malała powodując zmniejszenie granicy plastyczności stopu.

Przebadano wpływ długotrwałego starzenia w temperaturze 650°C na strukturę i własności. Starzenie przez 4000 godzin nie powodowało rozkładu fazy $Ni_2(Mo,Cr)$. Odkształcenie plastyczne przed starzeniem znacznie przyspieszało rozkład tej fazy na mieszaninę faz typu Ni_3Mo i Ni_4Mo.

Stwierdzono, że przy stosunkowo niewielkich odkształceniach obecność wydzieleń fazy $Ni_2(Mo,Cr)$ zmienia mechanizm odkształcenia plastycznego z poślizgu na mechaniczne bliźniakowanie. Rozwój struktury i tekstury krystalograficznej podczas odkształcenia nie zależy istotnie od wielkości wydzieleń i jest typowym dla metali o strukturze A1 i małej energii błędu ułożenia.

Przebadano wpływ temperatury, szybkości odkształcenia i atmosfery na własności mechaniczne wyznaczane w próbie rozciągania. Stwierdzono, że długotrwałe wyżarzanie przy 650°C prowadziło do wzrostu wielkości wydzieleń powodując wzrost wytrzymałości zarówno przy temperaturze pokojowej jak i 650°C. Wzrostowi wytrzymałości towarzyszył spadek plastyczności, szczególnie silny w temperaturze 650°C. Znaczny spadek plastyczności przy temperaturze 650°C był spowodowany oddziaływaniem atmosfery.

1. Introduction

Utilization of a long range order as a primary mechanism for providing enhanced elevated temperature strength in commercial wrought nickel-based alloys is a relatively recent development. The development of the significant long range order in nickel-chromium-molybdenum alloys following long exposure at intermediate temperatures, with an attendant increase in elevated temperature strength, has been a well known phenomenon for some time. It is only in the last 10 years, however, that compositions in the nickel-chromium-molybdenum system have been identified which allow the strengthening associated with the formation of these long range domains to be achieved with commercially viable aging times.

HAYNES®242™ alloy is one of such material. Since its commercial introduction in the early 1990's, 242 alloy has been selected for a variety of gas turbine engine component applications, many of which are made from forged or rolled rings. From the onset of production-scale reforge billet and ring manufacturing, the alloy has exhibited a marked sensitivity of its property response to a seemingly small degree of normal thermomechanical processing variability. This has been particularly the case

for elevated temperature tensile properties, for which extremes of high strength/low ductility and high ductility/low strength have been observed. Also, its behavior after long-term exposure at typical service temperatures has not been investigated in a systematic way yet.

In the present work, efforts have been made to characterize comprehensively the nature of long range ordering and secondary phase reactions in an attempt to provide the fundamental understanding of structure/properties interactions in this unique alloy. In particular, an emphasis was put on the influence of pre-aging modifications of heat treatment on ordering reaction, and linkage of the structural observations back directly to the observed mechanical property effects. Another purpose was to examine the influence of the ordered phase on microstructure and texture developing upon deformation (cold rolling) and *vice versa* the influence of the deformation microstructure on precipitation of new phases. Also, our goal was to examine the microstructure stability during long-term exposure (4000 hours) at typical sevice temperature (close to 650°C) and how such long-term exposure influences mechanical properties and deformation microstructures.

2. Influence of chemistry and heat treatment on microstructure

Chemistry. The challenge in the development of 242 alloy was twofold: to obtain a stable long-range ordered (LRO) phase, with a relatively high order to disorder transformation temperature, which did not degenerate into any detrimental phases, and to accelerate the kinetics of long range ordering transformation. These objectives were achieved by determinig the critical ranges of nickel, molybdenum and chromium as well as other minor elements. However, in certain proportions, molybdenum promotes long-range ordering reactions which result in the formation of phases detrimental to ductility, *e.g.*, Ni_4Mo and Ni_3Mo as in the Hastelloy alloy B. Also, molybdenum and chromium, in certain proportions, promote the formation of the μ and σ phases which also embrittle the alloy. Therefore, it was important to achieve a balance between molybdenum and chromium. The chemical composition of 25 wt.% molybdenum and 8 wt.% chromium, with nickel as a base circumvented these problems. The alloy contains also some impurities as carbon (up to 0.01 wt.%), iron (up to 1 wt.%), manganese (up to 0.5 wt.%), silicon (up to 0.4 wt.%), aluminum (up to 0.2 wt.%) and boron (about 0.003 wt.%).

Conventional aging. In the standard (conventional) heat treatment, 242 alloy is annealed at temperatures 1065°C to 1095°C and then water quenched. The aging treatment is carried out at 650°C for 24 to 72 hours in order to develop the long-range-order strengthening.

The effect of aging cannot be discerned by optical metallography, however, TEM investigation reveals the rapid formation of very small long range ordered domains with the Ni_2Mo (with Cr as a solute element) stoichiometry, very similar to those which have previously been observed to form in nominally Ni–16 wt.% Cr–16 wt.%

Mo-type alloys following hundreds of hours of aging [1]. The domains exhibit a lenticular shape, similar to that of γ'' particles in 718 alloy [2], with a typical initial long axis dimension of about 10—20 nm (Fig. 1a). Selected area diffraction (SAD) patterns taken from specimens containing the ordered phase exhibit extra reflections in addition to the f.c.c. reflections (Fig. 1b). The extra reflections appear at every $^1/_3<220>$ and $^1/_3<420>$ reciprocal lattice vectors. Some extra spots on the SAD patterns were streaked along $<210>$ directions. The SAD patterns confirm that the ordered domains constitute the Ni_2Mo phase. The crystallography of this phase was described by D a s and T h o m a s [3] and also by K u m a r and V a s u d e v a n [4, 5]. The atomic arrangement has been found to be isomorphous with the ordered

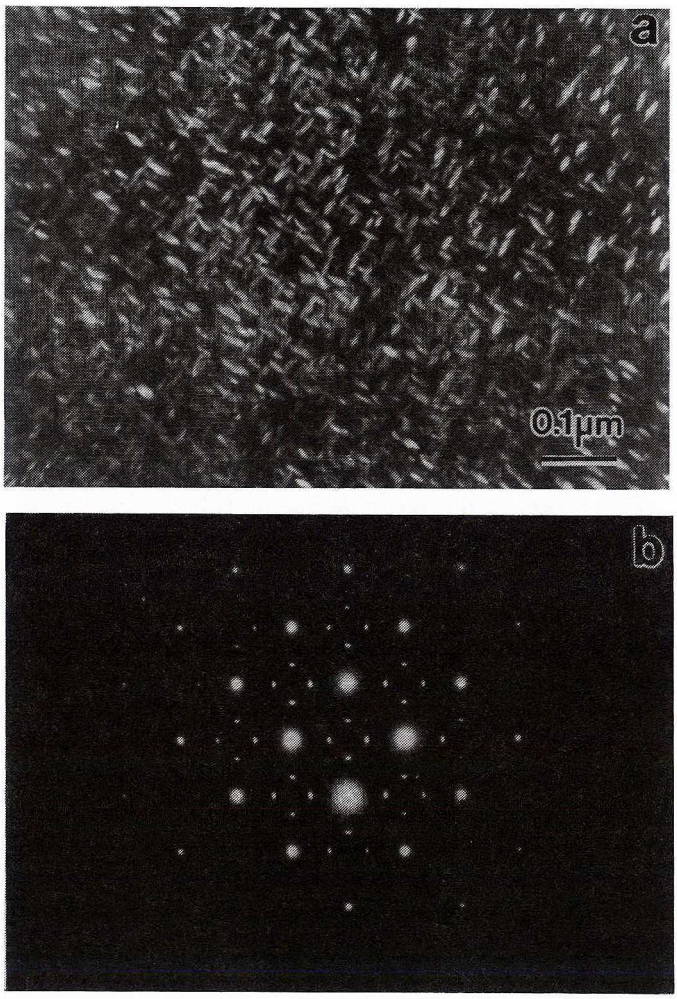

Fig. 1a. Typical Dark Field image of the ordered particles, (b) corresponding SAD pattern. (A relatively large objective aperture used in the dark field procedure allowed all four reflections from the ordered phase to contribute to the image of four, out of six possible, sets of the particles' orientations)

Pt_2Mo with the body-centered orthorombic unit cell. The relationships between the disordered f.c.c. lattice and the orthorombic Ni_2Mo lattice are: $[100]_o \| [110]_{fcc}$, $[010]_o \| [\bar{1}10]_{fcc}$, $[001]_o \| [001]_{fcc}$. This structure can be described by the stacking of atoms on either {420} or {220} planes where every third plane contains all Mo atoms and Ni atoms in between. Thus the reciprocal lattice of the ordered structure can be constructed from the original f.c.c. lattice, where the superlattice reflections appear at every $^1/_3<220>$ or $^1/_3<420>$ reciprocal lattice vectors. This gives rise to six orientation variants of the Ni_2Mo corresponding to six variants of {220} planes because of the two-fold degeneracy associated with stacking on {420} planes.

The ordered precipitates after conventional aging are too small to produce their own peaks on the *X*-ray spectra (despite their relatively large volume fraction), but they broaden the matrix peaks indicating the presence of coherency strains due to ordering (compare Figs. 2a and 2b).

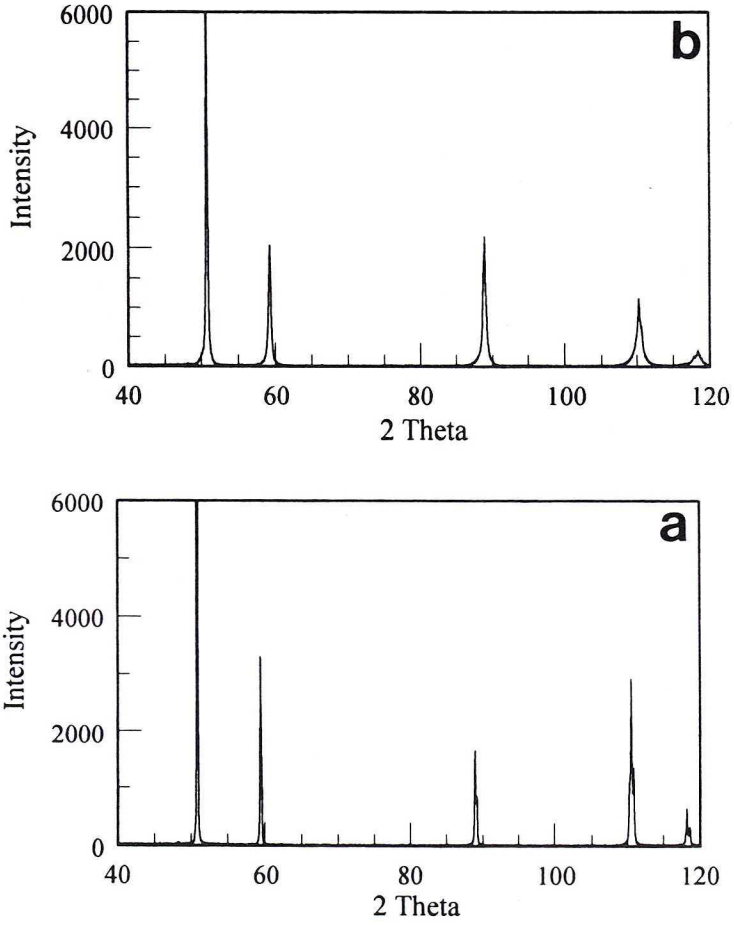

Fig. 2. *X*-ray spectra of selected samples: a) annealed material, b) conventionally heat treated material

The investigation of ordering kinetics has shown that the aging temperature as well as aging times affect the size and shape of the ordered precipitates. At temperatures above 500°C, the precipitates coarsen slowly and their length increases when the time of aging increases. Loss of long range order (and strengthening) appears to take place about 760°C, although domains have been observed to persist at slightly higher temperatures for a short exposure time. Instead, short--range-ordering, manifested on SAD patterns by strong diffuse intensity maxima at positions (1, $^1/_2$, 0), replaces long-range-ordering reaction.

In addition, the simultaneous effect of the amount of deformation and the annealing temperature (at constant time of 24 hours) on hardness was established for the as-annealed material. The results are collected in table 1. It appears that the hardness peak shifts toward lower temperatures when the amount of pre-aging deformation increases. This shows that the deformation accelerates the ordering reaction.

TABLE 1

Hardness of the as-annealed material deformed and subsequently annealed for 24 hours at various temperatures (HV10)

°C	0%	20%	40%	60%	80%
20	227	388	436	483	510
500	209	396	490	566	647
550	203	442	554	607	681
600	271	479	580	**625**	**706**
625	297	**531**	**595**	602	684
650	**383**	464	538	566	658
675	328	427	500	542	554
700	257	393	463	478	495
750	203	334	370	355	380

Maximum hardness is shown in bold.

Long-term aging. The long-term aging for 4000 hours at 650°C produces an order of magnitude larger precipitates (above 200 nm in length and about 40 nm in diameter) comparing to precipitates after conventional aging (Fig. 3). The large size of the ordered domains enabled chemical composition evaluation to be carry out by the XEDS. Such evaluation was performed on very thin areas close to the edge of the examined thin foil. The results are shown in table 2.

The molybdenum content in an ordered domain was about 35 wt.% while that in the matrix only 25%. Surprisingly, the chromium content did not differ notably between matrix and the ordered domains. The molybdenum content of 35 wt.%

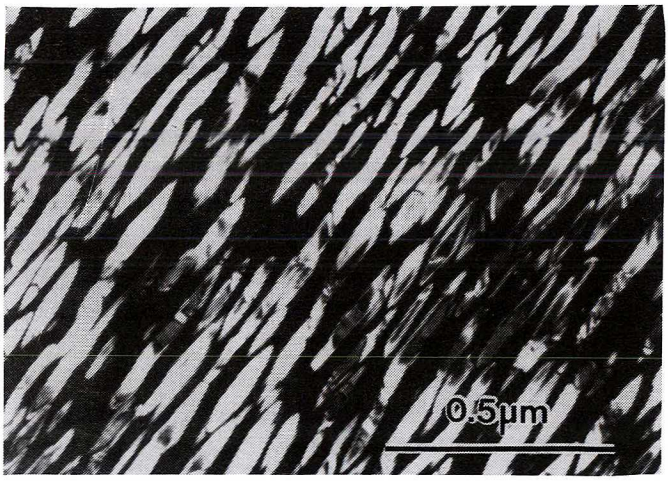

Fig. 3. Dark field image of the ordered domains after aging at 650°C for 4000 h

TABLE 2

Results of the XEDS analysis *

Element	Matrix		Ordered Domain	
	weight %	atomic %	weight %	atomic %
Cr K	8	11	8	10
Ni K	67	73	57	66
Mo L	25	16	35	24

* The amount of elements totals 100% (standardless technique)

(24 at.%) and the nickel content of 57 wt.% (66 at. %) suggest that Cr atoms substitute Mo atoms in the Ni_2Mo compound, so the stoichiometry of the ordered phase may be approximated by the $Ni_2(Mo,Cr)$.

Phase stability. As far as the stability of the ordered $Ni_2(Mo,Cr)$ is concerned, the Ni_2Mo phase in the binary Ni–Mo system is a metastable one [6, 7] while the Ni_2Cr phase in the binary Ni–Cr system is the stable one [8]. Thus, one can speculate that Cr stabilizes the $Ni_2(Mo,Cr)$ phase, however this phase does not appear on ternary Ni–Mo–Cr system diagrams [9, 10]. In order to investigate the stability of the ordered phase, the material (unaged, conventionally aged at 650°C/24 h and long-term aged at 650°C/4000 h) was cold rolled to 70 and 80% reduction followed by aging at 550°C and 650°C for 1000 hours. The plastic deformation in this case was believed to hasten the precipitation of equilibrium phases. The results unambiguously showed a tremendous change in microstructure with a new, needle-shaped, phase (phases) as a dominant feature. The *X*-ray spectra showed additional peaks corresponding to the Ni_4Mo and Ni_3Mo-type phases (Fig. 4).

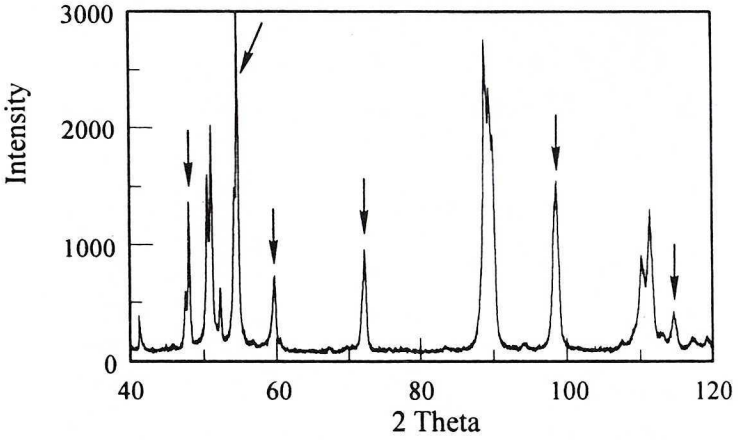

Fig. 4. X-ray spectrum of the sample aged for 4000 hours, cold rolled to 70% reduction and annealed at 650°C for 1000 hours; peaks from the Ni_3Mo phase are marked by arrows

The amount of the new phases depended strongly on the pre-deformation condition. The typical microstructures observed in SEM utilizing the contrast from backscattered electrons are shown in Fig. 5. The least amount of the Ni_3Mo-type phase was found in unaged samples annealed at 550°C. It appeared only in the former shear bands. On the other hand, the sample aged for 4000 hours before deformation contained the largest amount of this phase — almost entire structure contained needle or plate-like precipitates. Samples aged for 24 hours and deformed to 80% reduction contained less amount of this phase. It is characteristic that the new phases originated mainly in areas of highly localized deformation, *i.e.* within shear bands. In the regions with

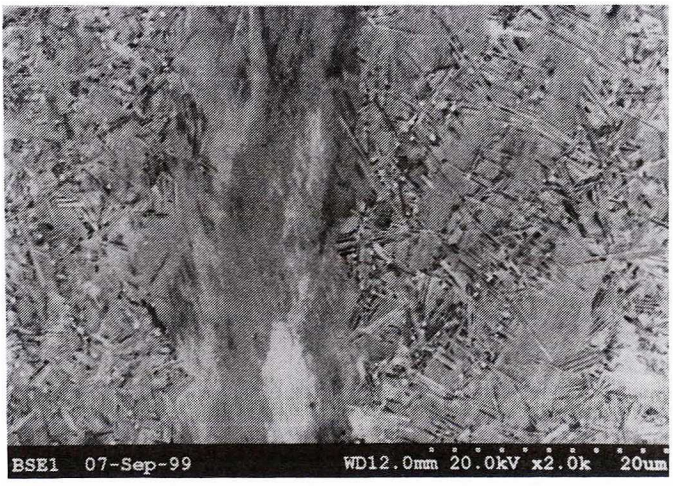

Fig. 5. SEM backscattered image of the microstructure of the conventionally aged then cold rolled sample to 80% reduction and subsequently annealed at 650°C for 1000 hours

uniform dislocation structure the new phases did not nucleate. The TEM investigation revealed that the Ni_3Mo-type phase contained large number of microtwins and stacking faults (Fig. 6). The molybdenum content in the new phases, established by the XEDS analysis (in TEM), varied within broad limits which cover compositions corresponding to the both Ni_4Mo and Ni_3Mo phases. Tne SAD patterns confirmed that the new phases are of the Ni_4Mo and Ni_3Mo type. The results of this experiment allow us to formulate a conclusion that the $Ni_2(Mo,Cr)$ phase is metastable and after very long annealing times transforms to the mixture of $Ni_4(Mo,Cr)$ and $Ni_3(Mo,Cr)$ phases.

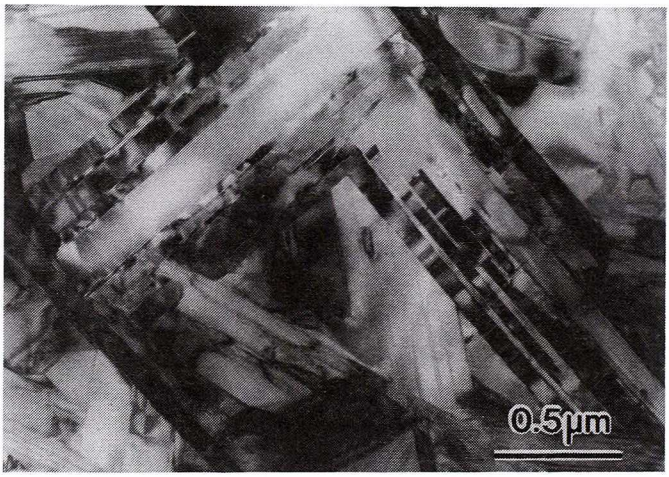

Fig. 6. TEM image of new phases in deformed and annealed for 1000 hours sample

Intermediate heat treatment. As was mentioned in the introduction, the 242 alloy is very sensitive to the thermomechanical processing conditions. In order to investigate this problem, the alloy (solution treated and quenched) was subjected to an intermediate heat treatment (IHT) before the final aging. The IHT comprised annealing for 4 hours at 760°C, 815°C, 870°C, 925°C and 980°C temperatures. The final aging at 650°C was conducted for 72 hours. This intermediate annealing showed, surprisingly enough, that the average particle size * depends strongly on the temperature of the intermediate heat treatment.

The aging of the intermediate heat treated samples produces larger precipitates than conventional aging. The largest domains were found after IHT at 760°C. The increase in IHT temperature makes the domain size to decrease. At temperature 980°C, the domains' size is almost the same as in the alloy not

* The average particle size was measured on dark field images. As a measure of the ordered particles' size the arithmetic mean of average lengths of precipitates' shorter and longer axes was used. To reduce errors, all measurements were carried out on the dark field images taken in the same reflection — $^1/_3$ $[3\bar{1}1]$, when the zone axis was [112].

subjected to the intermediate heat treatment (Fig. 7). It is believed that the short range ordering (SRO) developed during IHT is the reason of the variation in the ordered domain size.

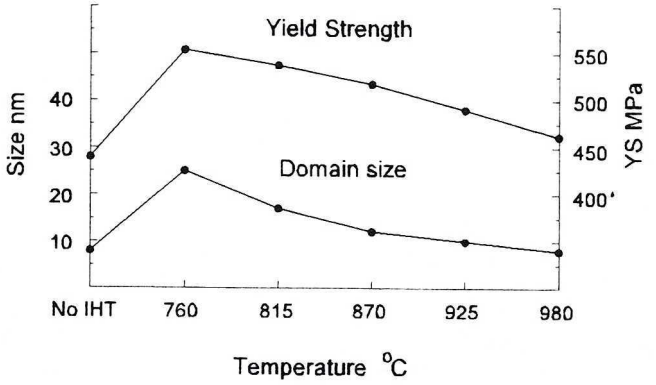

Fig. 7. Dependence of the ordered particles' size and the yield strength of the alloy on the IHT temperatures

In addition to the long range ordered domains, precipitation of other particles took place during IHTs. Two types of particles were observed: (1) round particles with no preferential nucleation sites, found both at grain boundaries and in grain interiors; (2) nearly continuous, or elongated and fragmented particles at grain boundaries. Continuous and/or elongated particles at grain boundaries are shown in Fig. 8. The amount and morphology, but not composition and crystallography of particles, change with the IHT temperature. Their morphology changes from nearly

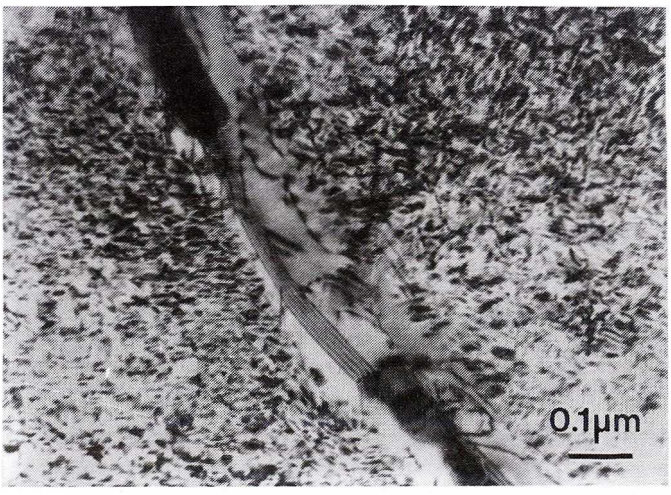

Fig. 8. Typical precipitates on a grain boundary in a sample subjected to the intermediate heat treatment

continuous (760–870°C) to elongated and fragmented (980°C). Their amount increases when IHT temperature increases from 760°C to 870°C and then decreases with IHT temperature increasing to 980°C.

The particles were indentified using SAD patterns and XEDS spectra. XEDS investigation revealed a broad spread in the chemical composition of the examined particles ranging from 50 to 65 wt.% of Mo, however, most particles contained about 50–55 wt.% Mo. The content of chromium in all particles was similar to that in the matrix. The precipitates which are expected in this alloy are the M_6C carbides with cubic crystal structure and the μ phase with hexagonal structure [11–14]. Neither phase has the precise stoichiometric composition and it is difficult to identify them unambiguously by the XEDS analysis alone. Therefore, the identification of these phases was accomplished by comparing the type of their SAD patterns which exhibit different symmetry (regular *vs.* hexagonal) and could be easy distinguished.

The formation of the μ phase in this alloy may seem unexpected since it does not occur in the three binaries of the Ni–Mo–Cr system, *i.e.* the Ni–Mo, Ni–Cr and Mo–Cr systems*. However, the μ phase was found in the Ni–Mo–Cr system as a ternary compound [14]. The μ phase reported by R a g h a v a n et al. [14] for Ni–Mo–Cr alloys was found to be stable over a wide range of alloy compositions. The μ phase contains usually 50–56 wt.% Mo and 10–20 wt.% Cr depending on the alloy composition. Alloys containing 25 and 30 wt.% Mo contained about 55 wt.% of Mo, the amount which was also found in the present study. The study on the samples which were cold worked up to 80% reduction in thickness and subsequently annealed at 850 and 900°C may pertain to the present discussion. The plastic deformation in this case accelerated the precipitation of the μ phase. The *X*-ray spectrum from so treated alloy revealed well-defined peaks of a hexagonal phase. The lattice parameters calculated from this spectrum were: a = b = 4.7558 Å (±0.0009), c = 25.6529 Å (±0.0053) and they were very closed to values given by G o z l a n et al. [15] for the μ phase found in other Ni–Cr–Mo alloys. The values were used to calculate the interplanar distances for the μ phase in the 242 alloy; the distances are comparable to those calculated from the SAD patterns. This unambiguously confirms the presence of the μ phase in the 242 alloy.

The type of carbides usually encountered in nickel-base alloys are $M_{12}C$ or M_6C [16, 17]. Both of them are called the η (eta) carbides. The selected area diffraction patterns from the carbides found in the examined alloy, obtained at different specimen tilt, prove that their crystallographic structure corresponds to the f.c.c. diamond type lattice. The lattice parameter of the M_6C carbide is 11.161–11.255 Å [16] (depending on composition) while it is 10.89 Å for the $M_{12}C$ [17]. The interplanar spacings calculated on the basis of these SAD patterns correspond roughly to the M_6C carbide. Though lattice parameter measurements using SAD patterns are not precise the lattice parameter found in our investigation was

* The formation of the μ phase has been reported in Fe–W, Fe–Mo, Co–Mo and Co–W binary systems with a A_7B_6 stoichiometry [14].

above 11 Å even when assuming a large experimental error. The compositions of the analyzed particles obtained by XEDS were: 51 – 54 at.% Mo, 35 – 37 at.% Ni and 10 – 11 at.% Cr. According to F r a k e r *et al.* [16] the ratio Mo : Ni from the range of 1.4 to 1.5 matches the composition established for the M_6C carbide. Whereas, the same composition ratio for the $M_{12}C$ carbide should be approximatelly 1 : 1 [18]. The content of chromium in such carbides was almost the same as that in the matrix. The results of the XEDS and SAD analyses lead to a conclusion that the particles found are unequivocally M_6C carbides. However, the presence of the $M_{12}C$ carbides can not be ruled out since only a small fraction of particle population was investigated.

Large number of particles of secondary phases (larger than after conventional aging) was observed also in samples aged for 4000 hours. The density and an average size of these particles were apparently greater than that in not-aged or aged for 24 h specimens. Usually, the particles were found at grain boundaries. Most of them was identified as carbides but the hexagonal μ phase was also found occasionally. Neither size nor shape dependence was found for these two classes of particles. However, unlike in the samples subjected to the IHT, where the μ phase was the dominant one, in the long-term aged samples at 650°C the majority of particles was identified as carbides.

Yet another interesting result of the investigation of samples subjected to the IHT is apparent dependence of the volume fraction as well as particle size of the ordered phase on the molybdenum content. The supposition that the chemical composition controls the volume fraction (and also the size) of the ordered phase can be concluded from the examination of grain boundaries in samples subjected to the IHT at the temperature range 760 – 870°C. Grain boundaries were decorated by precipitates of a second phase (Figs 8, 9, 10) in all samples treated at this temperature range. All figures show zones developing along grain boundaries, up to 0.5 μm wide, denuded of ordered particles. Dark field images show that the ordered particle size decreases and their volume fraction increases with the distance from the grain boundary (Figs. 9, 10). In the denuded zones, molybdenum content measured by the XEDS was about 22 wt.% and increased towards the grain interiors reaching the value characteristic of the matrix, between 25 and 26 wt.%. Thus, the lowering of molybdenum content leads to the formation of larger, but more loosely distributed, ordered domains. In the immediate vicinity of grain boundaries, no ordered particles were formed indicating that there is a critical molybdenum content below which no precipitation of the ordered phase occurs. It is worth to point out that SAD patterns from such areas show well defined extra spots corresponding to short ordered domains (indicated by arrows in Fig. 9). The depletion in molybdenum is caused by the precipitation of grain boundary particles which has been already discussed. The same order-domain-free zones were also found around round precipitates in grain interiors. The phenomenon of some elements (mainly Cr and Mo) depletion in the vicinity of precipitates was first recognized in austenitic stainless steels where led to the breakdown in corrosion resistance [19].

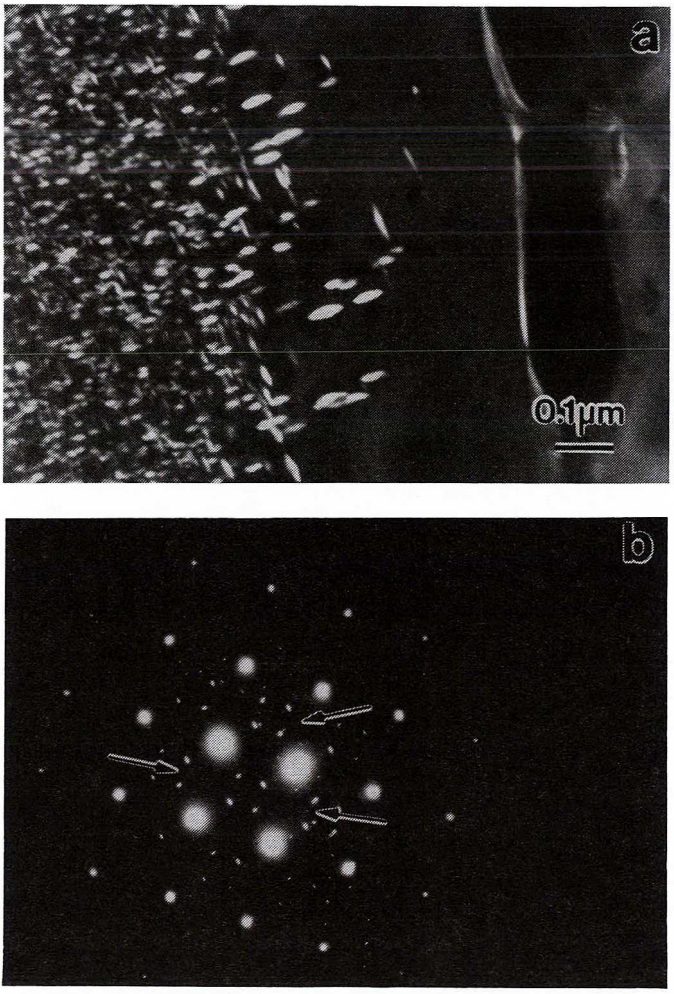

Fig. 9(a). Dark field image of a zone denuded of ordered domains around grain boundary precipitates, (b) corresponding SAD pattern; arrows show SRO reflections

The another evidence supporting the premise that the enrichment in Mo leads to an increase in the volume fraction of the ordered phase is provided by the described below observation. In samples subjected to IHT at temperature 980°C, large, approximately equiaxial carbides were occasionally found in the vicinity of which the volume fraction of the ordered phase was apparently higher than in more distant areas (Fig. 11). The molybdenum content close to the carbides was determined to be higher than far away from the carbides. For example, for the sample depicted in Fig. 11 the molybdenum content close to and far away from the carbide was determined to be: 29 wt.% and 26 wt.%, respectively. The higher concentration of Mo in this case is driven by higher temperature which is high enough to make carbides to dissolve and ease diffusion of Mo atoms away from precipitates.

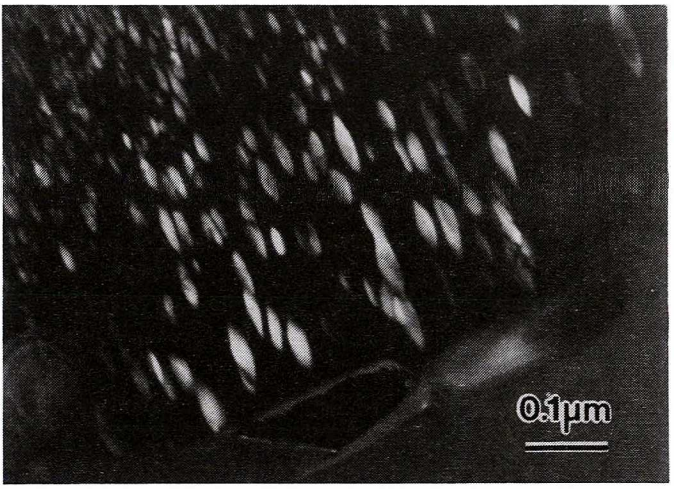

Fig. 10. A microphotograph illustrating how the long-range domain size changes with the distance from a grain boundary; dark field image

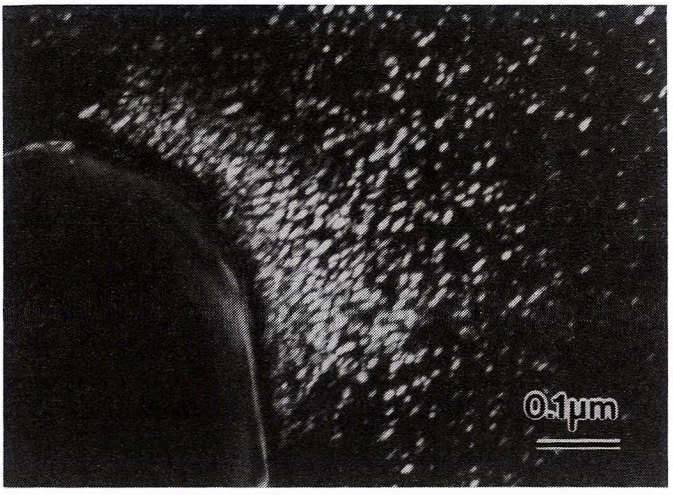

Fig. 11. Increased density of ordered phase domains close to a big particle in samples after aging of intermediately heat treated sample at 980°C

These observations show that the molybdenum content is the critical factor influencing the morphology and amount of the ordered phase in this alloy.

3. Mechanical properties

Mechanical properties were established from tensile tests for samples subjected to different variants of heat treatment. The tests were conducted at room and elevated

temperatures (up to 800°C) and with different strain rates. To address the influence of environment some tests were conducted in argon and vacuum.

Yield and tensile strength along with the elongation and reduction in area, measured in tensile tests at room and 650°C temperatures, for annealed, conventionally aged, and long-term aged specimens are collected in table 3. The data

TABLE 3

Mechanical properties of the examined alloy after different heat treatments tested in air at room and 650°C temperatures, strain rate $\dot{\varepsilon} = 8 \cdot 10^{-4} s^{-1}$

Aging time	Yield Strength [MPa]		Tensile Strength [MPa]		Elongation [%]		Reduction in Area [%]	
	20°C	650°C	20°C	650°C	20°C	650°C	20°C	650°C
0	435	345	952	883	59	53	76	40
24	828	565	1311	980	37	31	49	30
4000	911	737	1456	910	33	6	48	6

confirm that aging at 650°C for 24 hours results in an optimum combination of mechanical properties. At room temperature the yield strength of the material aged at 650°C almost doubles that of the unaged material and a relatively high room temperature ductility is maintained. This strengthening is accompanied by a modest reduction in ductility, as might be expected. The increase in strength is attributable to the observed long-range ordering.

Environmental embrittlement. The environmental embrittlement was observed at temperatures around 650°C for all examined alloy conditions but it was especially severe for the alloy aged for 4000 hours where large ordered precipitates were found. Thus this phenomenon will be discussed for the long-term aged condition. Tables 3 and 4 show the tensile properties for specimens tested in air at various temperatures at a constant strain rate of $8 \cdot 10^{-4} s^{-1}$ while tables 5 and 6 show the tensile properties for the long-term aged specimens tested in various environments and at various strain rates.

The data in table 3 show that the examined alloy is significantly stronger at both 20 and 650°C after the conventional aging than in the annealed condition. The 650°C strength of the alloy, though lower that that at the room temperature, is respectably high. The precipitation strengthening is accompanied by a reduction in ductility, but for all practical purposes the alloy still exhibits high ductility. The prolonged aging further strengthens the alloy, more than doubling its yield strength in the annealed condition. The prolongation of aging does not significantly affect the alloy's ductility at room temperature, but dramatically reduces it at 650°C. Such a dramatic deterioration of the alloy's ductility was also observed in the tensile tests conducted at the temperatures ranging from 550°C to 750°C (table 4) as well as in the 650°C tensile tests carried out in argon (table 5). On the other hand, when a specimen was tested at 650°C in vacuum the material exhibited ductility comparable with that of

TABLE 4

Mechanical properties at various temperatures for samples aged for 4000 hours and tested in air at the strain rate $\dot{\varepsilon} = 8 \cdot 10^{-4} s^{-1}$

Temp. [°C]	YS [MPa]	TS [MPa]	El. [%]	RA [%]
500	776	1220	28	54
550	775	1182	12	10
600	755	1005	6	6
650	737	910	6	6
700	635	838	6	6
750	368	715	9	9
775	375	548	82	80
800	345	477	92	67

TABLE 5

Mechanical properties at 650°C for samples aged for 4000 hours and tested in various environments

Environment	YS [MPa]	TS [MPa]	El. [%]	RA [%]
Air	737	910	6	6
Argon	720	845	7	5
Vacuum	686	1104	34	52

TABLE 6

Mechanical properties at 650°C for samples aged for 4000 hours and tested at various strain rates

Strain rate [s^{-1}]	YS [MPa]	TS [MPa]	El. [%]	RA [%]
$\dot{\varepsilon} = 8 \cdot 10^{-6}$	666	839	9	5
$\dot{\varepsilon} = 8 \cdot 10^{-4}$	737	910	6	6
$\dot{\varepsilon} = 8 \cdot 10^{-2}$	731	1152	26	17

the conventionally aged material. The deterioration of the alloy's 650°C ductility in the long-term aged condition was observed in the tests carried out at the lower strain rates of $8 \cdot 10^{-6}$ and $8 \cdot 10^{-4}$ s^{-1}, but not at $8 \cdot 10^{-2}$ s^{-1} (table 6).

The analysis of the data shown in tables 3–6 indicates that the dramatic deterioration of the Haynes 242 alloy's ductility, decreasing its elongation and reduction of area to below about 10%, was observed in the long-term aged condition, in the specimens tested at 650°C in air or argon, and at relatively low

strain rates. The drop of ductility was also observed in the tensile tests conducted in air at temperatures ranging from 550°C to 750°C. On the other hand, only a slight reduction in ductility was observed in the specimens in the annealed and conventionally aged conditions. After the prolonged aging, the ductility drop was absent in the specimens tested in vacuum at 650°C and in the specimens tested below 550°C and above 750°C.

The SEM observations indicate that the reduction in ductility is associated with a transition from ductle, dimple-type, to intergranular fracture (Fig. 12). All samples tested at 650°C exhibited similar appearance of fracture surfaces: in each specimen a part of the fracture surface is typical ductile (dimple type) and the other part is brittle (intergranular type). The brittle parts were always located close to the

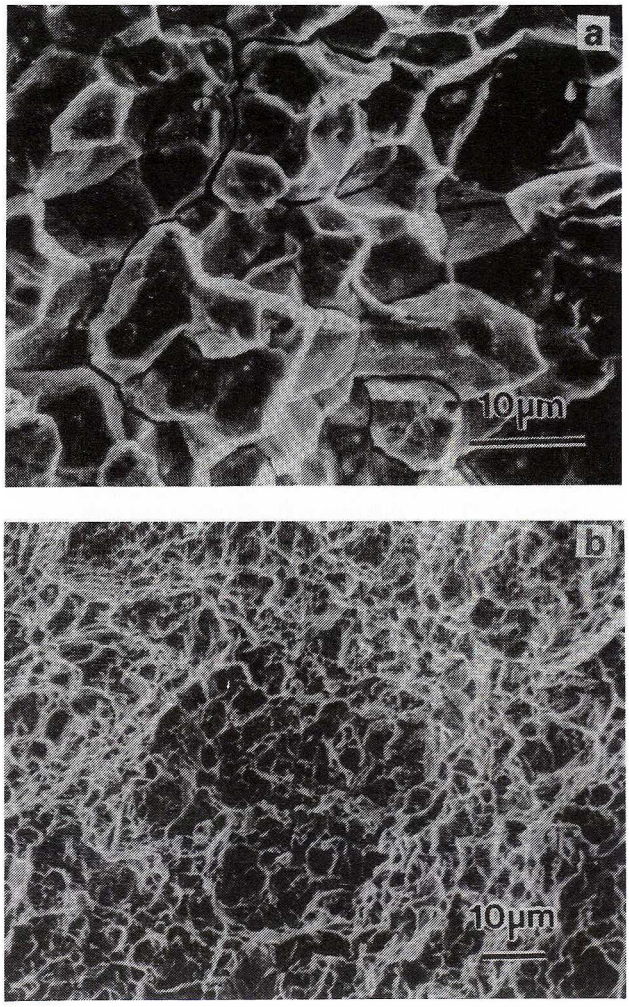

Fig. 12. Typical fracture surfaces in the specimen aged for 4000 h and deformed at 650°C: a) area close to the free surface, b) area close to the center

specimens' free surfaces. The extent of the intergranular fracture depends on the specimens' condition: the annealed specimens exhibit almost entirely ductile fracture (the intergranualar fracture occurs only locally in the very vicinity of the free surfaces) while in the specimens aged for 4000 hours the brittle portion was the largest. The fracture surface of the specimen tested at 775°C was fully ductile. As far as the influence of the strain rate is concerned, the specimens tested at the lowest strain rate broke almost entirely in a brittle manner while in specimens tested with the highest strain rate the ductile type of fracture was prevalent. Exemplary fracture surfaces of the long-term aged specimens deformed at 650°C are shown in Fig. 12. The fact that the areas of brittle fracture were found in the vicinity of specimens' surfaces provides yet another indication of the influence of the test environment.

Since, as the TEM observations and hardness measurements indicate, the long-range ordering in the alloy occurs in the temperature range between 550°C to 750°C, the embrittlement is related to the presence of ordered domains. Since the deterioration of ductility was observed in the long-term aged condition, but was insignificant in the conventionally aged condition, the increased size and volume fraction of the ordered domains appears to be a prerequisite for the embrittlement. However, even in the long-term aged condition the embrittlement was not observed when the specimens were tested in vacuum and this observation points to the influence of the test environment on ductility.

The TEM investigation showed that in the microstructure of the long-term aged specimens, deformed between 550°C and 750°C, exhibiting extensive brittle fracture and embrittlement, large ordered precipitates were observed while in the specimens deformed at 775°C the ordered phase was completely dissolved and the diffraction patterns did not exhibit superlattice reflections (Fig. 13). This points to the ordering reaction as the source of the embrittlement.

The exposure to air at 650°C itself, even for 4000 hours, does not affect the room temperature ductility significantly. Thus, the embrittlement is not caused by oxidation during aging such as the formation of oxide scales nor internal grain boundary oxidation, as might be expected. Instead, the embrittlement is clearly a dynamic effect occurring during elevated temperature tests, similar to that found in many intermetalic compounds [20–23]. It was also observed in other nickel-based superalloys (*e.g.* IN903A [24] and alloy 718 [2, 25]) not necessary subjected to prolonged aging.

The embrittlement in the Ni–Mo–Cr alloy is of the same type that the embrittlement found and analyzed by L i u et. al. [21, 22] in the boron doped Ni_3Al. According to L i u [22], the mechanism of the dynamic embrittlement involves several stages: (1) adsorption of oxygen molecules at crack tips where a high localized stress field is involved, (2) dissociation of molecules to form atomic oxygen, (3) oxygen diffusion to the stress field in front of tips, and (4) growth of cracks from the surface inward. As suggested by L i u [22], atomic oxygen weakens atomic bonds across grain boundaries. Though such effect was reported in some superalloys, *e. g.*, IN 903A [24], it is particularly severe in intermetalic phases. In the present study, the

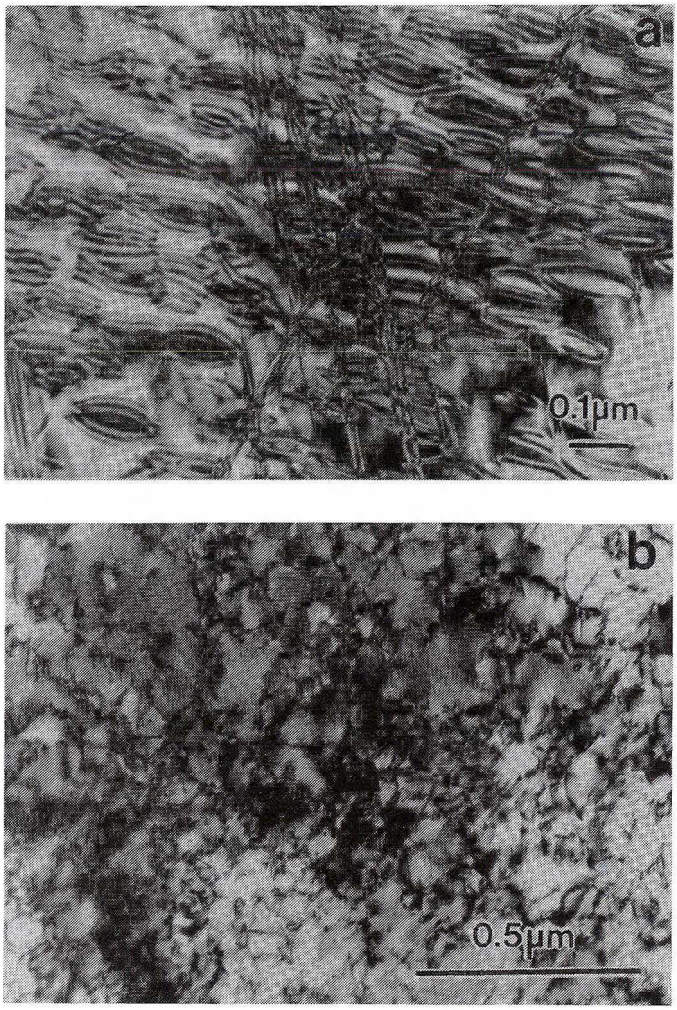

Fig. 13. Typical microstructure in samples deformed to failure: a) at 750°C (ordered precipitates, mechanical twins, b) at 775°C (no precipitates, dislocations)

brittleness at 750°C and an excellent ductility at 775°C, when the alloy is in a disordered state, suggests that the embrittlement is inherently associated with the presence of the intermetalic phase which presumably produces changes in the grain boundary structure. However, these changes must be confined to an atomic scale (bonding) since they were not detected by the TEM investigation.

Low ductility in the specimen tested in argon suggests that merely minute amount of at least one of the component of air, most likely oxygen, present in argon as an impurity is enough to cause the embrittlement. Also, the observation that at the high strain rate of $8 \cdot 10^{-2}$ s^{-1} the ductility drop is significantly smaller than in the tests conducted at the slower strain rates further rationalizes the role of the

environment on the dynamic embrittlement: simply, at the high strain rates it is difficult for the chemical reactions taking place at crack tips to keep up with growing cracks.

Influence of Intermediate Heat Treatment. As might be expected from the analysis of ordered domain size and precipitation of secondary phases produced by the IHTs, the tensile properties also depend on the temperature of the IHT. Room temperature mechanical properties of the examined samples are collected in table 7 and the yield strength dependance on the ordered domain size is depicted in Fig. 7.

TABLE 7

Mechanical properties at room temperature after different IHTs

Temperature of IHT °C	YS [MPa]	TS [MPa]	El. [%]	RA [%]
No IHT	440	874	48.0	56.5
760	553	927	33.2	39.0
815	537	854	22.9	27.9
870	517	827	23.6	25.2
925	490	852	28.7	34.0
980	462	848	32.2	36.3

The intermediate heat treatment at 760°C preceding aging significantly increases the yield and tensile strength of the aged alloy. The increasing temperature of the IHT gradually decreases the Haynes 242 alloy's strength and after the IHT at the highest temperature of 980°C the yield and tensile strengths differ only marginally — less than 5% — from the respective stresses in the material not subjected to the IHT. The strengthening caused by the IHT is accompanied, as might be expected, by a decrease of ductility but both the elongation to failure and reduction of area are still sufficiently high for technological applications. The reason of the ductility drop is apparently the discussed earlier precipitation of secondary phases on grain boundaries. The analysis of the results allows us to suggest that — within the range of the IHTs conducted in the present study — the IHT at 760°C for 4 hours preceding the conventional aging at 650°C for 72 hours optimizes the mechanical properties of the 242 alloy.

4. Deformation microstructure and texture

Tensile tested samples. Deformation microstructures were investigated on tensile tested as well as on cold rolled samples. In the unaged material (without ordered particles) plastic deformation was observed to occur through crystallographic glide on $\{111\}$ planes. Twinning occurred very seldom; twins were observed sporadically

in regions close to grain boundaries. Dislocations formed pile-ups and well-defined banded structure. Dislocations build up usually two sets of bands (dislocations rich layers), symmetrical to the tensile axis or to the rolling direction. Typical deformation structure of the unaged specimen deformed at room temperature is shown in Fig. 14.

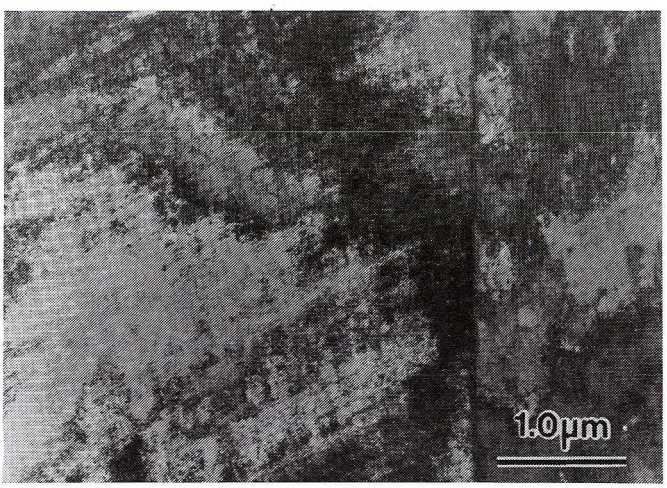

Fig. 14. Typical dislocation structure in an unaged sample tensile tested at room temperature

Microtwinning rather than crystallographic glide was observed to be predominant deformation mechanism in specimens containing ordered precipitates. Twinning occurred in one, two or even three systems depending on grain orientations (Fig. 15).

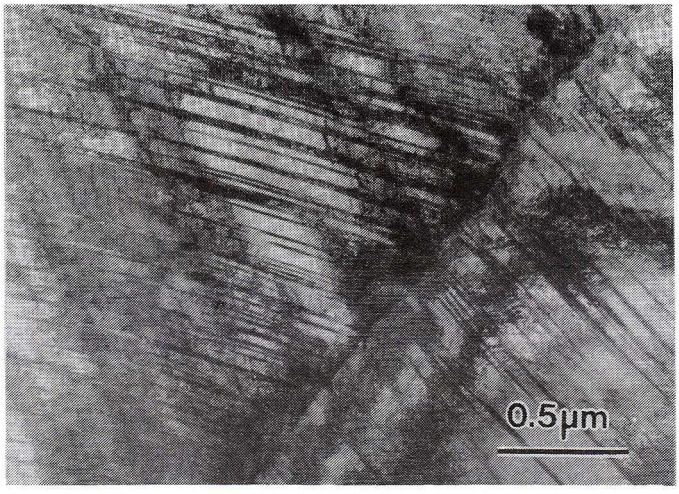

Fig. 15. Typical deformation twins in conventionally aged sample tensile tested at room temperature

In specimen aged at 760°C, where no ordered precipitates occurred, twinning almost ceased. Deformation occurred mainly by slip on {111} planes but deformation twins were found more often than in the unaged material, Dislocations were restricted to their slip planes. Sometimes stacking faults were visible.

After deformation of unaged specimens at elevated temperatures (350°C and 500°C), the banded structure became more distinct, dislocation structure was less uniform, occasionally microtwins occurred, but, by and large, the effect of temperature on deformation structure was not pronounced. The unusual occurrence of microtwins at elevated temperature may be associated with the strong tendency toward short or even long range ordering at elevated temperatures. The only difference was significant shearing of some grain and annealing twin boundaries, however, no structural inhomogeneities, such as microbands and shear bands, producing large shears were found. The selected area diffraction patterns from these samples showed typical f.c.c. reflections together with intensity maxima at different (1, $^1/_2$, 0) positions corresponding to short range ordered regions. Dark field images in the SRO reflections failed to reveal any microdomain structure. Aged specimens (650°C/24 h) tested at elevated temperatures deformed, as at room temperature, predominantly by twinning but mico-shear bands cutting deformation twins were occasionally found.

The phenomenon of changing deformation mode from slip to twinning was first attributed to the lowering of the stacking fault energy (SEE) [26]. Molybdenum is known to decrease the SEE of Ni-base alloys [27] and chromium is supposed to act in the opposite direction. However, the precipitation of the Ni_4Mo ordered phase in a binary Ni-19 at.%Mo alloy did lead to the change in deformation mode from slip to twinning [28], although the content of Mo in the matrix did not change considerably during precipitation, and the SFE of the matrix did not decrease. A semi-quantitative analysis of the present results also does not support the notion that the decreasing SFE of the matrix during ordering is the major factor encouraging the change of the deformation mode.

The change in deformation mode has been also discussed in the literature in terms of the effect of the structural change (f.c.c. → orthorombic) associated with ordering. It was shown what while such a change makes ten of twelve potential f.c.c. slip systems energetically unfavorable, it makes only two of twelve twining systems unfavorable [29].

In the light of the above discussion and the results of present TEM studies, we postulate that in the examined aged alloy slip occurs easily only in the early stages of plastic deformation [30]. After a few % elongation, dislocations pile-up on the slip planes that cause stresses to increase. Since dislocations cannot change their slip planes because ordered particles constitute strong obstacles for mobile dislocations and are known to restrict cross slip [31], the activation of other slip systems is unlikely. As a result, the alloy work hardens very strongly and the stress becomes high enough to activate twinning.

The fracture of unaged and aged specimens occurred by a cup and cone type of rupture. The fractographs taken from the unaged specimens, tested at room temperature, indicated that fracture was of the dimple type; fracture of the aged

specimens showed a change in the fracture mode from simple dimple type to a mixture of dimple rupture and cleavage [30].

Cold rolled samples. The differences in microstructure among deformed samples (after different pre-deformation heat treatments) studied by means of a light microscope were insignificant. TEM investigations confirmed previous observations made on tensile tested samples that aging at 650°C before deformation promotes much more intense twinning comparing to the unaged condition, however, deformation of unaged samples subjected to rolling produced more twins after the same amounts of deformation than in tensile tested samples. On the other hand, the material aged for 4000 hours deformed almost entirely by twinning (Fig. 16). Only in grains with the

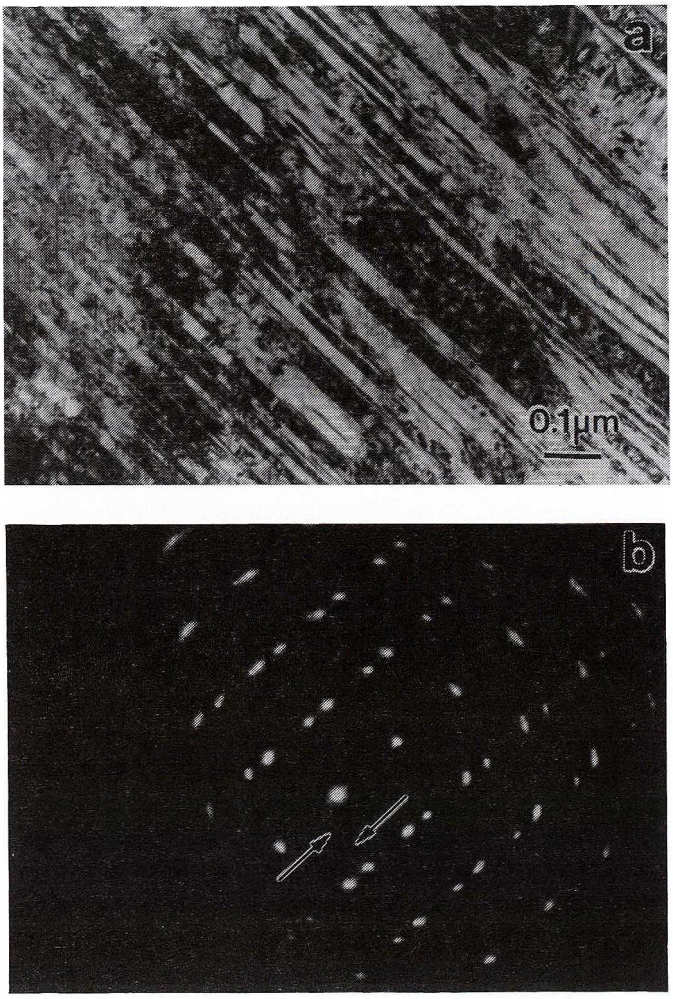

Fig. 16. Typical deformation twins in sample aged for 4000 hours and subjected to rolling with 70% reduction in thickness (a); the SAD pattern (b) shows extra spots from the $Ni_2(Mo,Cr)$ phase

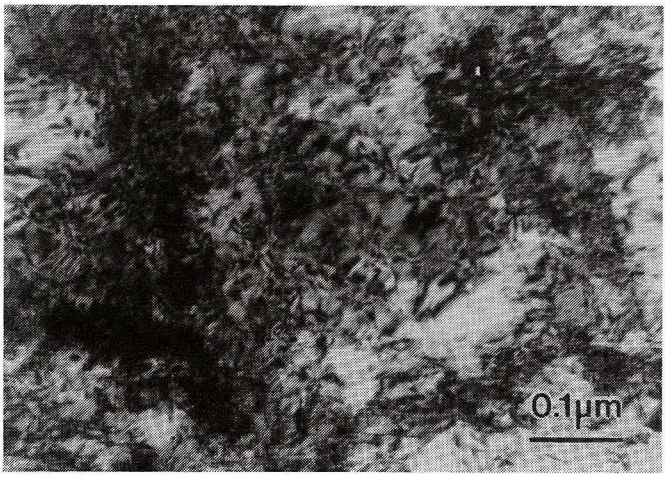

Fig. 17. The dislocation structure in a grain with the Goss orientation; deformation 70%, sample aged for 4000 hours

{110}<001> Goss orientation, even subjected to the highest applied amounts of deformation, the dislocation glide was the alone deformation mechanism (Fig. 17) — the observation consistent with other investigations carried out on dislocation microstructure of heavily deformed metals with low stacking fault energy [32]. Microstructure of samples rolled to lower reductions in thickness was relatively uniform but subsequent increase in the applied strain promoted inhomogeneous deformation. This was evidenced on TEM micrographs by a strong tendency toward localized deformation within shear bands (Fig. 18). Usually, shear bands were confined to a group of several grains but never crossed the entire section of the rolled bar. The $Ni_2(Mo,Cr)$ ordered phase was still detected in highly twinned regions but disappeared from shear bands. This was evidenced from SAD patterns which did not

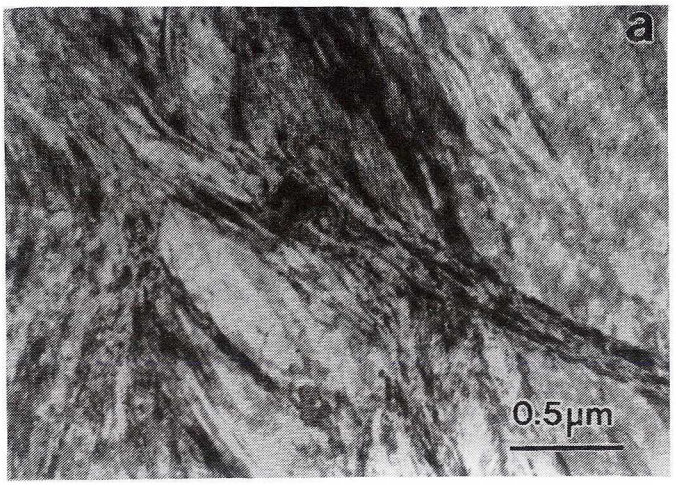

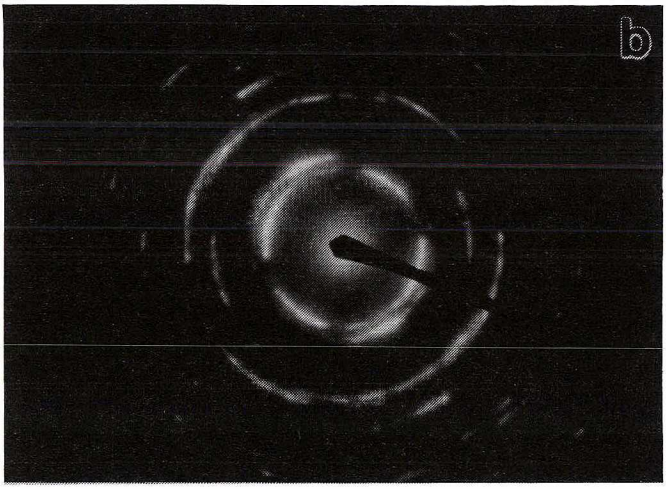

Fig. 18. Shear bands in a sample deformed to 70% by rolling; sample aged for 4000 hours (a) and corresponding SAD pattern (b)

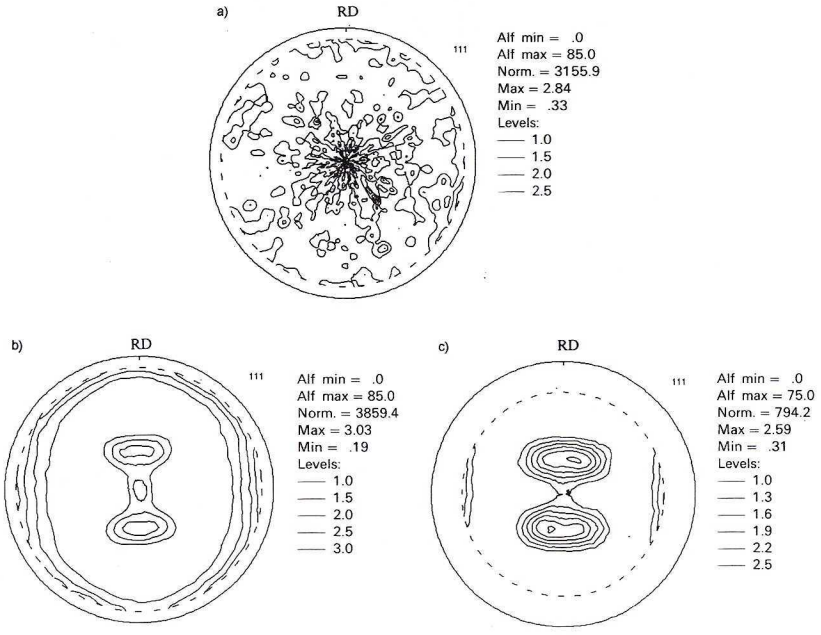

Fig. 19. {111} pole figures for a) undeformed sample, b) after 80% deformation of unaged sample, c) after 70% deformation for the sample aged for 4000 hours

show extra spots from the ordered phase. After highest reductions in thickness (70 and 80%) the well-defined shear bands crossing grain boundaries were a dominant feature of deformation microstructure. The overall deformation microstructure in the

examined alloy was typical for the microstructure found in other alloys with low stacking fault energy [32].

Texture measurements did not reveal any preferred orientation in the undeformed material but very strong texture after the highest amounts of deformation (Fig. 19). The deformation textures of all examined materials were similar regardless of the presence and size of the ordered precipitates before deformation. They were typical for f.c.c. metals with low stacking fault energy. After the highest amounts of deformation the {111} pole figure showed an orientation spread from the $\{110\}<001>$ orientation toward the $\{110\}<115>$ one. The raised intensity of poles in the center of the {111} pole figures points to the deformation twinning as a primary mechanism during heavy deformation of this alloy.

4. Conclusions

1. The dominant strenghthening mechanism in the aged 242 alloy is attributed to the formation of dispersed ordered $Ni_2(Mo,Cr)$ particles. The particles exhibit lenticular shape and size of 10–20 nm upon aging at 650°C for 24 to 72 hours (conventional aging). The precipitation of the $Ni_2(Mo,Cr)$ phase depends on molybdenum content in the matrix: When the molybdenum content in the matrix is below 24 wt.% ordering reactions are unlikley to occur. With increased molybdenum content the volume fraction of the ordered domains increases.

2. The long-term exposure to air at 650°C leads to the coarsening of ordered domains, increasing the alloy's room temperature and 650°C strength and reducing marginally its room temperature ductility. In the tensile tests carried out at 650°C a dramatic deterioration of the long-term aged alloy's ductility occurs. The embrittlement is observed in the temperature range corresponding to the occurrence of the coarse ordered domains. The embrittlement does not occur in the tests carried out in vacuum, so it is an environmentally-assisted, dynamic effect associated with the presence of the coarse ordered domains in the long-term aged alloy.

3. Aging for 4000 hours does not cause decomposition of the $Ni_2(Mo,Cr)$ metastable phase but plastic deformation followed by additional annealing at 650°C for 1000 hours makes the ordered phase to decompose on the mixture of stable Ni_3Mo and Ni_4Mo-type phases. Plastic deformation hasten, in this case, the formation of equilibrium phases.

4. The annealing at temperatures between 760°C and 980°C preceding conventional aging affects ordering reactions, grain boundary precipitation and mechanical properties of the Haynes 242 Ni–Mo–Cr alloy. The size of the ordered domains produced during final aging depends on the temperature of such intermediate heat treatment. The largest domains occur after annealing at 760°C, then, with the increase in temperature, the domain size decreases. The yield strength of the alloy increases with increasing particle size. The intermediate annealing produces detrimental to ductility the μ phase.

5. The presence of the ordered phase changes the deformation mechanism from slip into twinning.

6. The overall deformation substructure as well as deformation texture is not influenced by the ordered particle size.

Acknowledgments

The authors would like to thank Haynes Int. for conducting some variants of heat treatments and part of tensile tests as well as providing the material for the present study. We would like also to thank Drs. M. Rothman and D. Klarstrom for many fruitful discussion. The financial support from the Polish Committe for Scientific Research, grant No. 7T08A 042 12, is greatly appreciated.

REFERENCES

[1] H. M. Tawanacy, Met. Trans. **11A,** 1764, (1980).
[2] M. Sundararaman, P. Mukhopadhyay, S. Banerjee, Acta Metall. **36,** 847 (1988).
[3] S. K. Das, G. Thomas, Phys. stat. sol. **21A,** 177 (1974).
[4] M. Kumar, V. K. Vasudevan, Acta Materialia **44,** 1591 (1996).
[5] M. Kumar, V. K. Vasudevan, Acta Materialia **44,** 3575 (1996).
[6] T. Taburi, K. Komatsu, M. Yamamoto, S. Nemo, Y. Mizbani, Trans. AIME **254,** 2348 (1969).
[7] C. R. Brooks, J. E. Spruiell, E. F. Stansbury, Int. Mat. Rev. **29,** 210 (1984).
[8] P. Nash, Bulletin of alloy phase diagrams **7,** 466 (1986).
[9] A. K. Jena, S. B. Rajendraprasad, K. P. Gupta, J. Alloy Phase Diagrams **5,** 164 (1989).
[10] Handbook of Ternary Alloy Phase Diagrams, ed. P. Villars, A. Price, H. Okamoto, ASM **7,** 9025 (1994).
[11] M. Kumar, V. K. Vasudevan, Acta Materialia **44,** 4865 (1996).
[12] S. Dymek, M. Dollar, M. Wróbel, M. Blicharski, Archives of Metallurgy **44,** 279 (1999).
[13] S. Dymek M. Wróbel, M. Blicharski, M. Gazdowicz, Proc. of X Int. Conf. on Electron Microscopy of Solids. Warsaw – Poland, Sept. 20 – 23, 1999, ed. by E. Jezierska and J. A. Kozubowski, Printing Press of the Jagiellonian University, Kraków 211 (1999).
[14] M. Raghavan, R. R. Mueller, G. A. Vaughn and S. Floreen, Metall. Trans. **15A,** 783 (1984).
[15] E. Gozlan, M. Bambereger, S. F. Dirnfeld, Mat. Sci. Eng. **A141,** 85 (1991).
[16] A. C. Fraker, H. H. Stadelmaier, Trans. AIME **245,** 847 (1969).
[17] J. M. Leitnaker, G. A. Potter, D. J. Bradley, J. C. Franklin, W. R. Laing, Metall. Trans. **9A,** 397 (1978).
[18] C. P. Heijwegen, G. D. Rieck, Metall. Trans. **4,** 2159 (1973).
[19] E. L. Hall, C. L. Briant, Metall. Trans. **15A,** 793 (1984).
[20] C. T. Liu, C. L. White, E. H. Lee, Scripta Metall. **19,** 1247 (1985).
[21] C. T. Liu, C. L. White, Acta Metall. **35,** 643 (1987).
[22] C. T. Liu, "Structural Intermetallics", ed. by R. Darolia, J. J. Lewandowski, C. T. Liu, P. L. Martin, D. B. Miracle, M. V. Nathal, TMS, 365 (1983).
[23] C. A. Hippsley, J. H. DeVan, Acta Metall. **37,** 1485 (1989).
[24] R. H. Bricknell, D. A. Woodford, Metall. Trans. **12A,** 1673 (1981).
[25] R. Molins, G. Hochstetter, J. C. Chassaigne, E. Andrieu, Acta Mater. **45,** 663 (1997).
[26] H. M. Tawancy, J. Mat. Sci. **16,** 2883 (1981).

[27] T. C. Tiearney, N. M. Abbas, N. J. Grant, Metall. Trans. **13A,** 1827 (1982).
[28] H. M. Tawancy, Abbas, J. Mat. Sci. **24,** 1845 (1989).
[29] P. D. Johnson, PhD thesis, University of Notre Dame, Indiana, 1980 (after Ref. [26]).
[30] S. Dymek, M. Dollar, Scripta Metall. **25,** 865 (1991).
[31] V. Gerold, H. P. Karnthaler, Acta Metall. **37,** 2177 (1989).
[32] M. Wróbel, S. Dymek, M. Blicharski, S. Gorczyca, Archives of Metallurgy **38,** 195 (1993).

REVIEWED BY: PROF. DR HAB. INŻ. BOGUSŁAW MAJOR

Received: 12 September 2000.